

## ENDOR study of an $O^-$ ion observed in x-ray-irradiated carbonated hydroxyapatite powders

P. Moens, F. Callens, S. Van Doorslaer, and P. Matthys

*Laboratory of Crystallography and Study of the Solid State, Krijgslaan 281-S1, B-9000 Gent, Belgium*

(Received 6 July 1995; revised manuscript received 18 September 1995)

A carbonated hydroxyapatite powder synthesized at high temperatures has been examined with electron paramagnetic resonance (EPR) and electron-nuclear double resonance (ENDOR). In the EPR spectra, an intense signal assigned to an  $O^-$  radical was observed. The interactions of the  $O^-$  radical with three inequivalent sets of  $^{31}\text{P}$  nuclei as well as with one set of protons were resolved in the ENDOR powder spectra. By a careful analysis of the ENDOR powder spectra using computer simulations based on the "orientation-selection principle," a detailed model for the  $O^-$  radical and its surroundings could be derived. In this way, it was established unambiguously that the  $O^-$  ion is located on a hydroxyl site. In addition, experimental evidence was found that the precursor of the  $O^-$  radical is a carbonate group, and not a hydroxyl group. Next to the  $O^-$  radical, EPR and ENDOR resonances of another paramagnetic center were observed. After analysis of the spectra and by comparing the results with previous work, this radical was assigned to a  $\text{CO}_3^{3-}$  ion located at a phosphate site.

### I. INTRODUCTION

The mineral hydroxyapatite,  $\text{Ca}_{10}(\text{PO}_4)_6(\text{OH})_2$ , forms the basic constituent of the so-called calcified tissues such as bone, dental enamel, etc. The demineralization process of these biological apatites is largely determined by the amount and the location of carbonate ions in the hydroxyapatite lattice.<sup>1</sup> As carbonate ions are always present as a major contamination, a study of the incorporation and location of carbonate ions in the apatitic lattice is obviously important. In the lattice, carbonate ions substitute for hydroxyl groups or phosphate groups, called *A* and *B* type substitutions, respectively. In addition, carbonate ions can be located at the surface of the apatite crystallites.<sup>1</sup>

In the past twenty years, several research groups attempted to obtain information about the location of some carbonate-derived radicals by using electron paramagnetic resonance (EPR) spectroscopy.<sup>2-18</sup> With this technique, it is in principle possible to deduce the nature of the paramagnetic species under study. The determination of the location of the radical in the host lattice however, is less evident, as the resolution of this technique in most cases is too low to allow for the determination of the superhyperfine interactions (interactions between the unpaired electron spin of the paramagnetic radical with the nuclear spins of the surrounding nuclei). Hence researchers tried to look for correlations between the EPR data and the results of, e.g., IR spectroscopy to obtain information about the location of the center. This, however, is far from obvious.<sup>12-18</sup>

In contrast to EPR, the resolution of the ENDOR technique (electron nuclear double resonance) is usually high enough to resolve the different superhyperfine interactions. If the corresponding EPR signals have appropriate saturation characteristics, the interaction of the radical with the surrounding nuclei can be studied quite profitably with ENDOR.<sup>19</sup> Within certain approximations, it is in principle possible to determine the type of the interacting nucleus and its location in the *g* tensor axes frame.<sup>20-23</sup> Hence detailed information about the environment of the paramagnetic cen-

ter, and thus the location of the species can be found.

In contrast to the extensive EPR literature, it is striking that only a few articles are published on ENDOR studies of carbonated hydroxyapatites, whether biological or synthetically prepared. Sato<sup>5</sup> recorded a structureless proton ENDOR signal while monitoring the anisotropic  $\text{CO}_2^-$  EPR signal in x-ray-irradiated powdered human tooth enamel. Van Willigen *et al.*<sup>24</sup> detected ENDOR resonances on the  $\text{CO}_2^-$  signal observed in human tooth enamel blocks. These authors recorded a broad  $^{31}\text{P}$  singlet and a  $^1\text{H}$  doublet form which they deduced that the nuclei had to be separated from the paramagnetic center by at least 0.6 and 0.9 nm, respectively. So they concluded that the radical had to be located on the surface of the apatite crystallites. In a recent publication, Moens *et al.*<sup>25</sup> performed ENDOR measurements on a  $\text{CO}_3^{3-}$  radical observed in synthetic hydroxyapatites. The ENDOR measurements substantiated a *B* site model for the  $\text{CO}_3^{3-}$  radical, with a vacancy on the nearest hydroxyl site. Very recently, the well-known isotropic  $\text{CO}_2^-$  signal at  $g=2.0007$ , often observed in precipitated apatites and attributed to a tumbling  $\text{CO}_2^-$  radical, was investigated with ENDOR.<sup>26</sup> It was concluded that the  $\text{CO}_2^-$  radical had to be located in the so-called "occluded water," i.e., a remnant of the aqueous solution from which the samples were precipitated, entrapped between the crystallites.

Thus, so far, ENDOR evidence has been presented for radicals located on a *B* site, a surface site and in the "occluded water." In the present paper, ENDOR evidence will be presented for an  $O^-$  ion located on an *A* site, i.e., substituting for a hydroxyl group. In addition, the nature of the precursor of the  $O^-$  ion will be discussed.

### II. THE PRINCIPLES OF POWDER ENDOR

The EPR spectra of polycrystalline materials reflect a powder average of all molecular orientations with respect to the applied magnetic field.<sup>27,28</sup> A molecular orientation is determined by a set of  $\theta$  and  $\phi$  angles defining the direction of the applied magnetic field vector in the *g* tensor axes frame.

In an ENDOR experiment, only a limited number of molecular orientations are selected as the magnetic field is kept fixed at a certain field value corresponding to an EPR resonance. This is often called the “orientation-selection” principle, introduced by Rist and Hyde.<sup>29</sup> For a system with  $S=1/2$  and  $I=1/2$  and for which the  $g$  tensor anisotropy is small compared to the averaged  $g$  value (which will be the case of interest here), general formulas for calculating the ENDOR frequencies at a given field value are given by several authors.<sup>20,21,25</sup> Assuming a pure point dipole-dipole interaction for the anisotropic superhyperfine interaction, the final expression for the ENDOR frequencies as a function of the applied magnetic field contains four unknown parameters, i.e.,  $\theta_N$  and  $\phi_N$ : the angles defining the direction of the interacting nucleus in the  $g$  tensor axes frame;  $r$ , the distance between the unpaired electron and nuclear spin and  $A_{\text{iso}}$ , the isotropic part of the superhyperfine interaction. For systems with an axial  $g$  tensor, the parameter  $\phi_N$  is superfluous. The use of the point dipole approximation to calculate the electron-nuclear spin distance is only valid if covalency effects are considered to be small, i.e., when the overlap between lattice ions and defect orbitals is negligible. Depending on the system, a lower limit for allowing the use of the point dipole approximation is between 0.3 and 0.4 nm.<sup>23</sup> For the system studied in this paper, this condition will be fulfilled.

For systems with a quasiaxial  $g$  tensor (as will be the case for the radical studied in this paper), fairly good begin estimates for the parameters  $A_{\text{iso}}$ ,  $r$ , and  $\theta_N$  can easily be obtained from the experimental ENDOR spectra in a way that is described in full detail by Moens *et al.*<sup>25</sup>

In short, the procedure is as follows (throughout it is assumed that the principal  $g$  tensor values are known from EPR measurements). ENDOR spectra are recorded for different magnetic field values. From the field value for which the largest splitting between two resonances (belonging to the same ENDOR doublet) is visible, the value for  $\theta_N$  can be calculated. This maximum splitting ( $\Delta\nu_1$ ), together with the splitting measured at the field value corresponding to  $\theta_N \pm 90^\circ$  ( $\Delta\nu_2$ ) gives rise to two equations with two parameters  $r$  and  $A_{\text{iso}}$ , which can readily be solved. The values thus obtained for the parameters  $A_{\text{iso}}$ ,  $r$ , and  $\theta_N$  are used as input parameters in the powder ENDOR simulation program “PENSIL.”<sup>25</sup> The value for the parameter  $\phi_N$  has to be estimated from a proposed model. Ultimately, the different parameters are optimized using an iterative procedure.<sup>25</sup> For systems with a nearly axial  $g$  tensor, the value of  $\phi_N$  has little effect on the simulated ENDOR powder spectra, hence the error on the value of this parameter can be quite large.

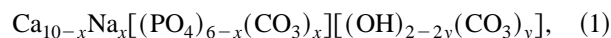
### III. MATERIALS AND METHODS

#### A. Materials

The hydroxyapatite lattice has a hexagonal structure. The space group is  $P6_3/m$ , with  $a=b=0.9432$  nm and  $c=0.6881$  nm. Hydroxyl groups are located on the hexagonal  $c$  axis whereas the phosphate groups are distributed as equilateral triangles around the hexagonal axis. The crystal structure is described in full detail by Kay *et al.*<sup>31</sup>

The sample studied in the present paper is a carbonated calciumapatite synthesized by sintering appropriate mixtures

of reagent grade  $\text{CaHPO}_4$ ,  $\text{CaCO}_3$ , and  $\text{Na}_2\text{CO}_3$  at high temperature. Full details of the preparation and the physical and chemical analysis of the sample are given by Driessens *et al.*<sup>30</sup> and will not be repeated here. The x-ray-diffraction pattern and the IR spectra show sharp and well-resolved peaks characteristic of well-crystalline solids. In the IR spectra absorptions due to  $A$ -type and  $B$ -type carbonate ions are detected. The sample also contains a certain amount of sodium ions, replacing  $\text{Ca}^{2+}$  ions in the apatite lattice. The stoichiometry of the sample is given by the following formula:<sup>30</sup>



with  $x=1.5$  and  $y=1.0$ .  $x$  and  $y$  are called the  $B$  and  $A$  type substitution parameters, respectively. Thus, according to the chemical analysis of the sample, all hydroxyl groups are replaced by carbonate ions.

#### B. Methods

The EPR spectra were recorded using a Bruker ESP300 X-band spectrometer, with a maximum microwave power of 200 mW. The magnetic field was modulated at 100 kHz with a peak-to-peak amplitude of  $0.5 \times 10^{-4}$  T. All the EPR spectra were normalized to the same frequency, i.e., 9.47 GHz and hence can be directly compared. Large normalization factors have been avoided.

The magnetic field was measured using a Bruker ER035M Gaussmeter. With this equipment it is possible to measure accurately the relative positions of the EPR signals present. Small shifts in the magnetic field positions down to  $0.1 \times 10^{-4}$  T can be detected. For absolute  $g$  value determination, a calibration using the  $g$  standard DPPH (diphenylpicrylhydrazyl) at 0.1 mW ( $g=2.0036$ ) was performed.

ENDOR spectra were recorded on the same spectrometer equipped with a Bruker ESP353E ENDOR/TRIPLE extension (EN374 RF amplifier with a maximum power of 200 W, EN525 Schomandl synthesizer, and an ER033M field frequency lock unit). The best ENDOR signals were obtained with a microwave power of 0.4 mW (27 dB) and 200 W radio frequency (rf) power (0 dB). The modulation depth was set to 100 kHz and ten scans of 81 s each were run for each ENDOR spectrum. The low temperatures necessary to saturate the EPR signals were realized using an Oxford ESR 10 flow cryostat.

The irradiation of the sample was performed using a tungsten anticathode Philips x-ray tube, operated at 60 kV and 40 mA, for 20 min. This corresponds to a dose of approximately 26 kGy.

### IV. EXPERIMENTAL RESULTS

#### A. EPR results

After x-ray irradiation, the sample exhibits strong EPR signals attributable mainly to two different paramagnetic species. Figure 1 shows a typical EPR spectrum recorded at room temperature. The labelling of the EPR signals is in agreement with previous work.<sup>12-18</sup> As can be seen from the figure, the two most intense EPR signals overlap in the region around  $g=2.00$ . Smaller resonances attributable to other centers are also visible in the same field region. In

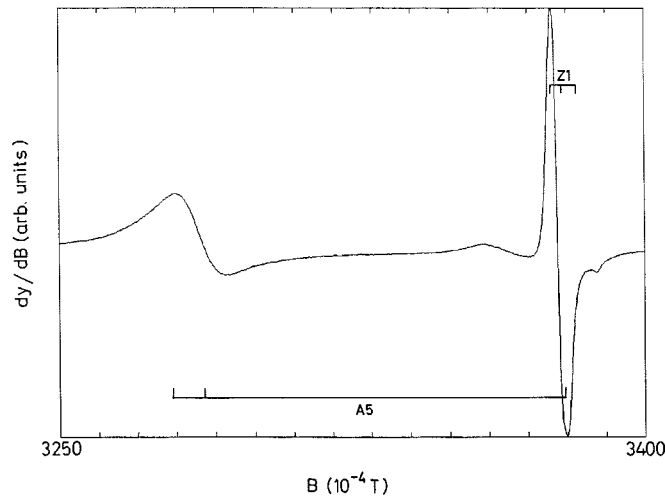


FIG. 1. A typical EPR spectrum, recorded at room temperature with a microwave power of 10 mW. The two most important components are indicated in the figure.

order to determine the  $g$  tensor values and linewidth parameters of the two most intense signals, an adequate spectrum decomposition technique has to be applied.<sup>32</sup> The spin Hamiltonian parameters thus obtained are summarized in Table I. Figure 2 shows the computer fittings of the isolated A5 and Z1 signals. It can be noticed from Table I that the A5 radical has an orthorhombic  $g$  tensor with only a small deviation from axial symmetry. So, to a first approximation, the  $g$  tensor of this defect is taken to be axial with  $g_{\perp} = 2.063 \pm 0.001$  and  $g_{\parallel} = 2.001 \pm 0.001$ . The error on the  $g$  values originates from the large linewidth of the EPR resonances in the  $g = 2.063$  region (unresolved superhyperfine interaction) and the overlap of the Z1 signal in the  $g = 2.001$  region.

In this paper only the A5 signal will be discussed in detail. This signal remains visible down to approximately 15 K, at lower temperatures, the A5 signal disappears from the EPR spectrum, i.e., it is completely saturated. On the other hand, the Z1 signal can still be observed at liquid helium temperatures. As a result, the A5 signal cannot be isolated experimentally by varying the temperature or the microwave power. The other small signals around  $g = 2.00$  (see Fig. 1) disappear from the spectrum at temperatures below 100 K.

### B. ENDOR results

In order to have sufficient microwave saturation, the specimen has to be cooled. The ENDOR resonances are visible from 15 K up to 60 K, with an optimum detection tem-

TABLE I.  $g$  tensor and linewidth parameters of the two most intense and isolated EPR signals as derived from the computer fittings. The error on the last digit is given between brackets.

Label	$g_x$	$g_y$	$g_z$	$\Delta B (10^{-4} \text{ T})$
A5	2.068(1)	2.058(1)	2.001(1)	$\Delta B_x = 6.9(3)$ $\Delta B_y = 5.6(3)$ $\Delta B_z = 4.1(2)$
Z1	2.0044(2)	2.0032(4)	2.0015(2)	1.5(1)

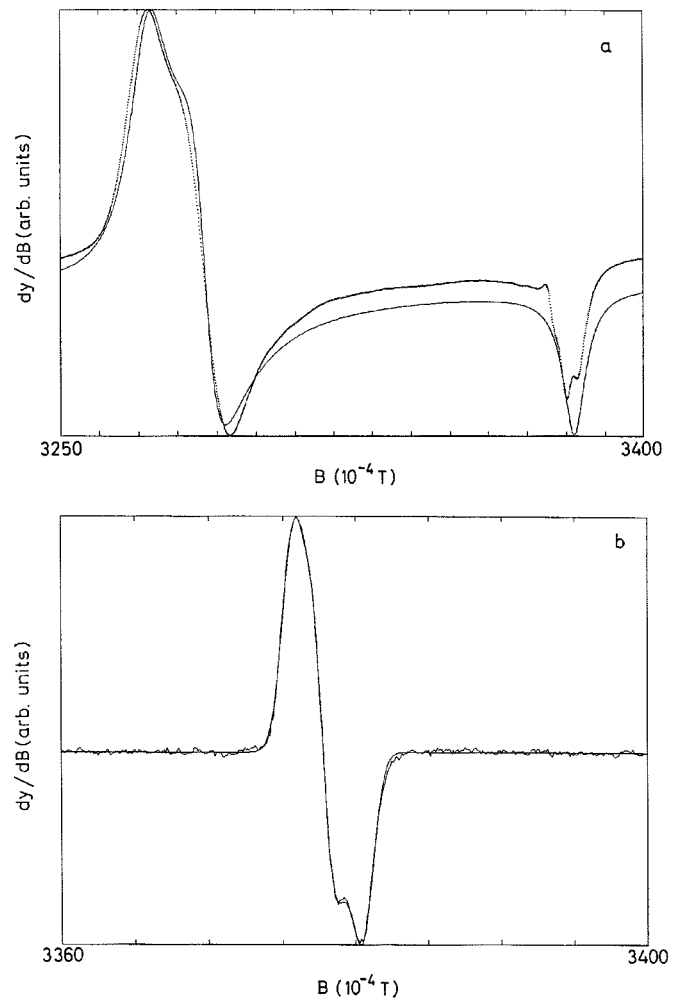


FIG. 2. Computer fittings of the isolated A5 (a) and Z1 (b) signals, at room temperature.

perature of 20 K. Unfortunately, at this temperature, the Z1 EPR signals still overlaps with the A5 signal in the region around  $g = 2.00$ .

A typical ENDOR spectrum is shown in Fig. 3. The

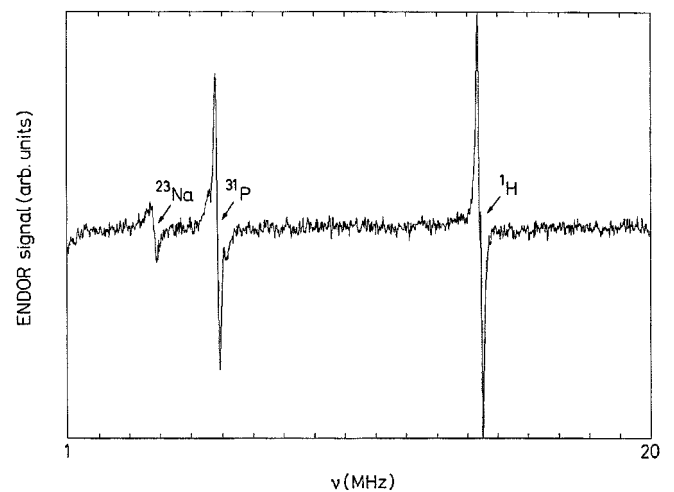


FIG. 3. A typical ENDOR powder spectrum recorded at 20 K. For the experimental conditions, see Sec. III B.

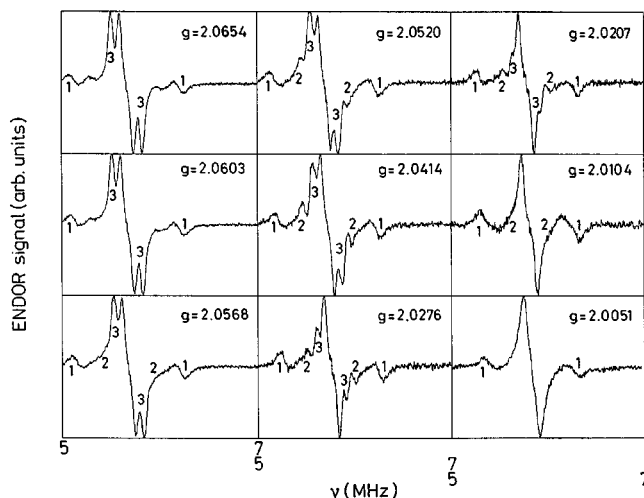


FIG. 4. Angular variation of the  $^{31}\text{P}$  hyperfine interactions. The different doublets are indicated in the figure ( $T=20\text{ K}$ ).

ENDOR spectrum consists of three sets of peaks centered around the nuclear Zeeman frequencies of  $^{23}\text{Na}$ ,  $^{31}\text{P}$ , and  $^1\text{H}$ , respectively. That  $^{23}\text{Na}$  interactions are observed is not surprising as we are dealing with a sodium containing hydroxyapatite specimen (see Sec. III A). Powder ENDOR spectra are recorded for nine different magnetic field settings within the EPR powder envelope, i.e., from  $g=2.0654$  to  $2.0051$ . For lower  $g$  values ( $g \cong g_z$ ; see Table I), ENDOR spectra are not recorded due to the overlap of the Z1 EPR signal. This will have almost no effect on the analysis and interpretation of the ENDOR spectra, as the  $g=2.0051$  position is already very close to the  $g_z$  direction (see Table I).

From the ENDOR experiments, it follows that for all magnetic field settings the  $^{23}\text{Na}$  resonances exhibit almost no spectral resolution, i.e., we are dealing with broad, unresolved lines. Most probably, this is related to the fact that the  $^{23}\text{Na}$  nucleus also exhibits quadrupole interaction, greatly increasing the complexity of an ENDOR powder spectrum.<sup>22</sup> Therefore, the  $^{23}\text{Na}$  interaction will not be discussed and hence only the angular variations of the  $^{31}\text{P}$  and  $^1\text{H}$  interactions are studied in detail.

### $^{31}\text{P}$ interaction

Figure 4 shows the angular variation of the  $^{31}\text{P}$  interactions. Several doublets, centered around the nuclear Zeeman frequency of  $^{31}\text{P}$ , are visible and indicated in the figure. Unfortunately, also a large matrix ENDOR signal attributable to distant  $^{31}\text{P}$  nuclei is present.

The resonances of doublet 1 exhibit the largest splitting. For all field settings these resonances are well resolved. The splitting is maximal for  $g=2.0654$  ( $\theta \cong 90^\circ$ ) and decreases slightly with increasing field value. The minimal splitting is observed for  $g=2.0051$  ( $\theta \cong 0^\circ$ ). Taking the  $g$  tensor to be axial ( $g_\perp=2.063$ ,  $g_\parallel=2.001$ ) one thus expects, according to the procedure outlined in Sec. II, that the  $^{31}\text{P}$  nuclei responsible for the interaction of doublet 1 are located in the plane perpendicular to  $g_\parallel$ . From the spectra at  $g=2.0654$  and  $g=2.0051$  one can obtain values for  $\Delta\nu_1$  and  $\Delta\nu_2$ , giving rise to initial estimates for the parameters  $A_{\text{iso}}$ ,  $r$ , and  $\theta_N$ . Using these values as input parameters in the PENSI program, re-

TABLE II. Distances, polar angles, and  $A_{\text{iso}}$  values for the different interactions as derived from the ENDOR spectra using a point dipole approximation. The errors are indicated between brackets.

Nucleus	Label	$A_{\text{iso}}$ (MHz)	$r$ (nm)	$\theta_N$	$\Phi_N$
$^{31}\text{P}$	<i>P1</i>	-0.20 (0.02)	0.35 (0.01)	85 (5)	40 (30)
$^{31}\text{P}$	<i>P2</i>	0.0 (0.05)	0.50 (0.02)	50 (10)	?
$^1\text{H}$	<i>H1</i>	-0.04 (0.02)	0.50 (0.02)	3 (3)	?

sults obtained after some iterations are given in Table II (interaction labeled *P1*). The EPR linewidth  $\Gamma_{\text{EPR}}$  is orientation dependent (see, e.g., Table I) and the ENDOR linewidth  $\Gamma_{\text{END}}$  is taken to be 70 kHz. In cases where the deviations from axial symmetry are small, the error on the  $\phi_N$  value can be quite large and hence these values have to be interpreted with caution. A theoretical powder ENDOR spectrum for doublet 1 simulated with the values of the parameters given above, is shown in Fig. 5 together with the corresponding experimental spectrum for one magnetic field setting. The reproduction of the resonance positions, the line shapes, and the intensities can be called quite satisfactory. The same quality of reproduction of the experimental spectra was obtained for all magnetic field settings.

The resonances of doublet 2 are largely hidden under the resonances of doublet 3 and the matrix ENDOR signal, making the analysis less straightforward. The splitting is largest for  $g \cong 2.041$ , which means that  $\theta_N \cong 50^\circ$ . The best simulations for doublet 2 are found by using the parameters given in Table II (interaction labeled *P2*). The values for the other parameters are the same as those used in the simulation of the resonances of doublet 1. The  $\phi_N$  value could not be determined from the spectra.

Doublet 3 is attributable to  $^{31}\text{P}$  nuclei located further away from the paramagnetic center. From the largest splitting, a minimum value for  $r$  of  $0.60 (\pm 0.04)$  nm is estimated.

### $^1\text{H}$ interaction

The angular variation of the  $^1\text{H}$  interaction is shown in Fig. 6. As can be seen from this figure, an intense matrix

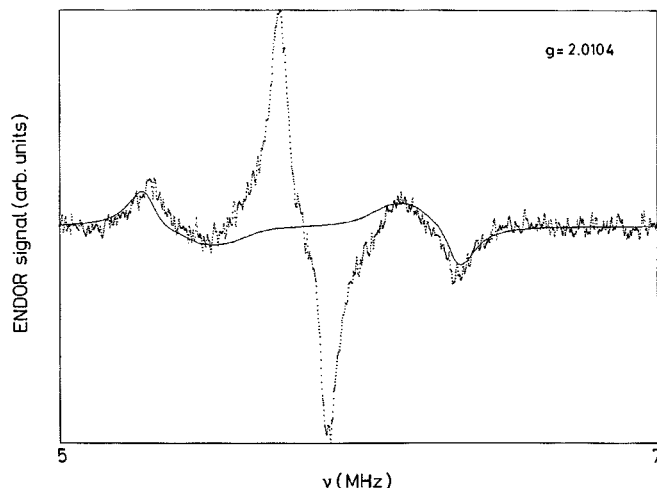


FIG. 5. Comparison between the experimental and simulated  $^{31}\text{P}$  ENDOR powder spectrum for the resonances of doublet 1, for one magnetic field setting ( $T=20\text{ K}$ ).

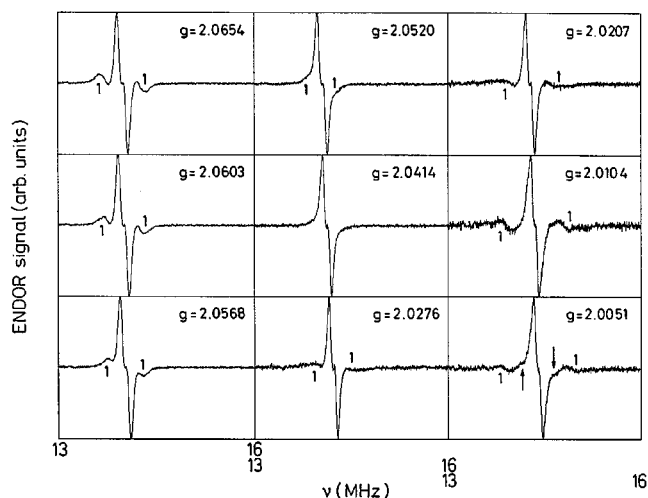


FIG. 6. Angular variation of the  $^1\text{H}$  ENDOR hyperfine interaction. The doublet is indicated in the figure. The arrows indicate the presence of another doublet ( $T=20$  K).

ENDOR signal is visible, together with the resonances of one doublet, the resonances of which are centered around the proton nuclear Zeeman frequency. The resonances of this doublet cross each other underneath the matrix ENDOR signal at  $g \cong 2.041$ . Their splitting is largest for  $g \cong g_{\parallel}$ , indicating that  $\theta_N \cong 0^\circ$ . Table II lists the parameters giving the best simulation of the experimental spectra. The value for  $\phi_N$  could not be determined. The values for the other parameters are the same as those used in the simulation of the  $^{31}\text{P}$  interactions. A simulated ENDOR powder spectrum together with the corresponding experimental spectrum is shown in Fig. 7, for one magnetic field value. Again, the agreement between the simulated and experimental spectra is quite reasonable. The quality of the fit shown in Fig. 7 is representative for all magnetic field settings.

## V. DISCUSSION

The two most important features to discuss are the nature and the site allocation of the A5 radical. They will be treated

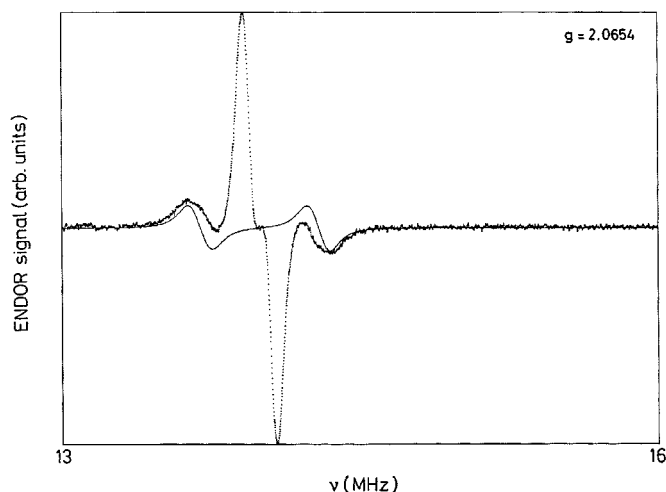


FIG. 7. Comparison between the experimental and simulated  $^1\text{H}$  ENDOR powder spectrum for the resonances of the proton doublet, for one magnetic field setting ( $T=20$  K).

TABLE III. Spin Hamiltonian parameters for  $\text{O}^-$  ions detected in irradiated hydroxyapatites.

	$g_x$	$g_y$	$g_z$
Single crystal <sup>a</sup>	2.0683	2.0683	2.0018
Powder <sup>b</sup>	2.066	2.066	?
Powder <sup>b</sup>	2.055	2.055	?
Powder <sup>c</sup>	2.068	2.058	2.001

<sup>a</sup>From Ref. 33.

<sup>b</sup>From Ref. 7.

<sup>c</sup>This work.

separately. The nature of the precursor of the A5 radical will also be discussed. In addition, the Z1 signal will be dealt with cursorily.

### A. The nature of the A5 radical

Considering its  $g$  tensor values only an  $\text{O}^-$  ion seems to be a plausible candidate for the A5 radical. A radical with very similar  $g$  tensor values has already been detected after x-ray irradiation in pure, i.e., carbonate-free, hydroxyapatite single crystals by Mengeot *et al.*<sup>33</sup> These authors substantiated that this radical has to be ascribed to an  $\text{O}^-$  ion originating from a hydroxyl group. Large proton superhyperfine interactions (of the order of 20 MHz) were resolved in the EPR spectrum. Two  $\text{O}^-$  ions have also been observed in synthetic hydroxyapatite powders synthesized at high temperatures.<sup>7</sup> One of these  $\text{O}^-$  spectra exhibited relatively strong proton superhyperfine interactions (doublet structure) whereas the other  $\text{O}^-$  radical did not (singlet structure). The singlet increased with increasing carbonate content of the samples whereas the doublet decreased, indicating a modification in the radical environment upon carbonation. Both radicals were located at A sites. Table III summarizes the different  $g$  tensor values as determined by Mengeot *et al.*<sup>33</sup> and Tochon-Danguy *et al.*,<sup>7</sup> together with the values we found for the A5 radical. The strong correspondence indicates that the A5 radical indeed has to be assigned to an  $\text{O}^-$  ion, most probably located at an A site.

### B. The location of the A5 radical

As no superhyperfine interactions were resolved in the EPR spectrum, the location of the  $\text{O}^-$  radical in the apatitic lattice has to be deduced from the ENDOR data.

From the striking correspondence between the  $g$  values of the A5 radical and the ones of an  $\text{O}^-$  radical detected in hydroxyapatite single crystals and located at an A site (superhyperfine interactions were visible in the EPR spectrum<sup>33</sup>), it is tempting to assume that the A5 radical is also located on an A site. Indeed, as will be shown below, the ENDOR data can only be explained by assuming an A site allocation for the  $\text{O}^-$  ion.

The model suggested for the A5 radical is shown in Fig. 8 and will be substantiated and elucidated further in the discussion. The  $p_z$  lobe, in which the unpaired electron of the  $\text{O}^-$  ion is residing, is assumed to be oriented parallel to the hexagonal  $c$  axis. According to the theory of the  $\text{O}^-$  ion,<sup>34</sup> the smallest  $g$  value ( $g_z \sim g_{\parallel}$ ) is measured along this direction. Following the model of Fig. 8, the nearest-neighboring

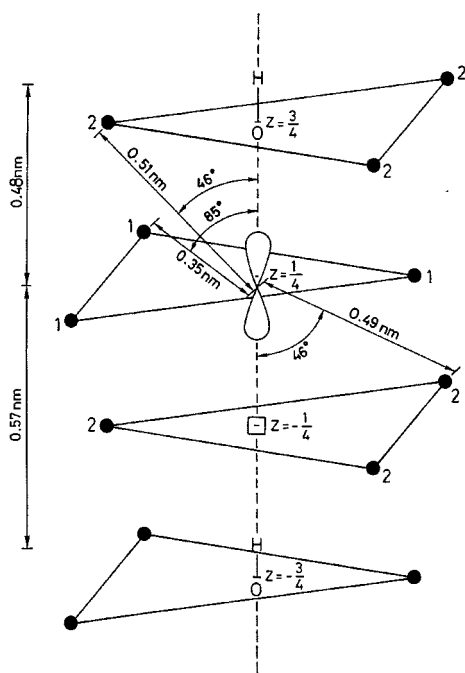


FIG. 8. Model for the relaxed  $O^-$  ion in hydroxyapatite as deduced from the EPR and ENDOR measurements. The paramagnetic  $p_z$  lobe of the  $O^-$  ion is oriented parallel to the hexagonal  $c$  axis. The indices 1 and 2 denote the phosphorus nuclei responsible for the resonances of doublets 1 and 2, respectively.

(NN) phosphorus nuclei are situated in the plane perpendicular to the  $g_{\parallel}$  axis ( $\theta_N \cong 90^\circ$ ) at a distance of 0.35 nm, as determined from neutron diffraction experiments.<sup>31</sup> These NN phosphorus nuclei are indicated in Fig. 8 with index 1. This is in nearly perfect agreement with the experimental values for the resonances of doublet 1, i.e.,  $\theta_N = 85^\circ$  and  $r = 0.35$  nm. For a nonaxial  $g$  tensor, the three phosphorus nuclei are not equivalent, but, as the deviation from axial symmetry for the  $O^-$  ion is small, the three phosphorus nuclei are considered to be equivalent.

The small deviation from  $90^\circ$  for the value of  $\theta_N$  might indicate that possibly the  $O^-$  ion is not exactly situated at its  $z = 1/4$  position, but somewhat above or below this lattice position. When calculating its out-of-equilibrium position, one comes to a value of 0.03 nm that the  $O^-$  ion should be relaxed.

The resonances of doublet 2 are attributable to the next-nearest-neighboring phosphorus nuclei (NNN). According to the crystal structure of hydroxyapatite, these are situated in the mirror planes just above and below the radical. The distance between the NNN phosphorus nuclei and the paramagnetic center, if not relaxed, is 0.50 nm whereas the angle between the  $g_{\parallel}$  axis ( $p_z$  lobe) and the direction connecting the electron and nuclear spins (i.e.,  $\theta_N$ ) is  $46^\circ$ .<sup>31</sup> These data are in very good agreement with the ENDOR results for doublet 2 ( $r = 0.50$  nm and  $\theta_N \cong 50^\circ$ ).

The small displacement of the  $O^-$  ion, necessary to explain the NN  $^{31}\text{P}$  interactions, will not influence these conclusions. The distances between the radical and the NNN nuclei will become 0.51 and 0.49 nm, regarding the nuclei are situated in the mirror plane above or below the  $O^-$  ion,

respectively. The  $\theta_N$  angles do not vary significantly. Thus all the values are within the uncertainty on the experimental data.

According to the analysis of the ENDOR resonances of doublet 3, the corresponding phosphorus nuclei have to be located at a distance larger than approximately 0.6 nm. This agrees with the crystal structure of hydroxyapatite according to which the phosphorus nuclei other than those labeled 1 and 2 are located at a minimum distance of 0.58 nm.

Following the model depicted in Fig. 8, the NN proton is situated along the  $c$  axis and thus  $\theta_N$  is expected to be approximately  $0^\circ$ . The distance of this proton to the unrelaxed  $O^-$  ion depends on the orientation of the nearby hydroxyl group. If the proton of this hydroxyl group is pointing away from the radical, the distance between both should be 0.45 nm.<sup>31</sup> On the other hand, when the proton is pointing towards the  $O^-$  ion, the distance should be 0.25 nm.<sup>31</sup> Another possibility is that the paramagnetic center is surrounded by two vacancies at the nearest hydroxyl sites. In this case, the nearest hydroxyl groups are located at a distance of 0.59 or 0.79 nm, dependent on the orientation of the proton. By comparing the value of  $r$  determined experimentally ( $r = 0.50$  nm) with the ones given above, it follows that only the model in which the proton of a nearby hydroxyl group points away from the radical agrees with the experimental data. The disagreement between the "model distance" and the "ENDOR distance," however, is 11%. This discrepancy can be lifted if it is again assumed that the  $O^-$  ion is not exactly placed at its  $z = 1/4$  position, as was already suggested in the discussion of the  $^{31}\text{P}$  interactions. An out-of-equilibrium distance of 0.03 nm (as was calculated from the  $^{31}\text{P}$  interactions) would make the "model distance" and the experimental distance to coincide within experimental error. In this case, however, a vacancy has to be present at a NN hydroxyl site because otherwise the proton of this hydroxyl group (at  $z = -1/4$ ) would be located at a distance of 0.42 or 0.22 nm, in contradiction with the experimental data. In addition, the presence of such a vacancy would allow the  $O^-$  ion to relax. The origin of this vacancy will be discussed in the next section.

According to the model (see Fig. 8), the NNN proton originates from the hydroxyl group at  $z = -3/4$ . If this proton is pointing towards the  $O^-$  ion, its distance should be 0.57 nm. Thus this proton should give rise to ENDOR resonances exhibiting the largest splitting for  $g = g_{\parallel}$  with a splitting of approximately 0.86 MHz. The ENDOR spectrum at  $g = 2.0051$  indeed reveals the presence of another doublet, as indicated by the arrows in Fig. 6. The splitting is estimated to be 0.75 MHz.

Thus the ENDOR data can be explained by assuming an A site allocation for the  $O^-$  ion. A B site allocation can be ruled out as in this case, the distance between the radical and the NN phosphorus nuclei should be 0.40 nm,<sup>31</sup> too large compared to the value of 0.35 found experimentally. Moreover, in the case of a B site allocation, the NN phosphorus nuclei and the NN protons should be situated almost in the same plane. This clearly is in contradiction with the experimental data, for which the NN phosphorus nuclei have  $\theta_N \cong 90^\circ$ , whereas for the NN protons  $\theta_N \cong 0^\circ$ . Hence a B site model for the  $O^-$  ion can be discarded.

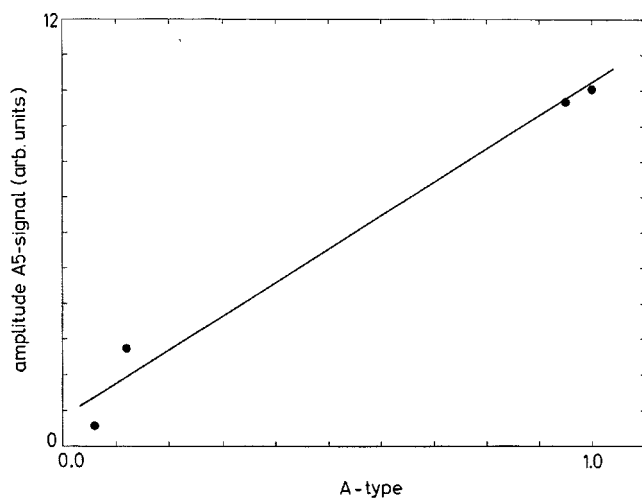


FIG. 9. Amplitude of the A5 EPR signal as a function of the A type substitution parameter  $\gamma$  (Ref. 30) of a series of related hydroxyapatite samples.

### C. The precursor of the $O^-$ radical

As the ENDOR studies unambiguously made clear that the  $O^-$  radical is located at an A site, only a hydroxyl or a carbonate group are plausible precursors for the  $O^-$  ion.

At first glance, it seems reasonable to assume that the  $O^-$  ion originates from a hydroxyl group from which the proton has been removed by x-ray irradiation. However, the two  $O^-$  ions already detected in hydroxyapatite single crystals<sup>33</sup> and powders<sup>7</sup> and which are assumed to originate from a hydroxyl group, exhibited large proton splittings, even observable in the EPR spectrum (doublet structure). Such a doublet structure was not detected in the EPR spectrum of our sample. On the other hand, the sample studied in this paper contains  $CO_3^{2-}$  ions substituting for hydroxyl groups. In addition, this sample originally made part of a series of four carbonated hydroxyapatites, each sample having a different carbonate content.<sup>12,13,30</sup> When the amplitude of the A5 EPR signal is plotted against the A type carbonate substitution parameter  $\gamma$  [see Eq. (1)] of each sample, a positive correlation is found, as is shown in Fig. 9. It has to be pointed out that in this figure, the differences in molecular weight of the samples are not taken into account. The errors thus introduced, however, are small (less than 5%) and hence do not alter the figure significantly. The pronounced positive correlation suggests a carbonate group as precursor for the  $O^-$  radical. Moreover, the introduction of a carbonate group on a hydroxyl site introduces a vacancy on the NN hydroxyl site, according to the following substitution mechanism:<sup>30</sup>

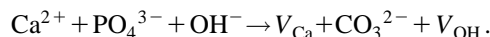


$V_x$  denotes a vacancy on a  $x$  lattice site. In this way, the appearance of the vacancy on the nearest hydroxyl site is explained. This vacancy is also depicted in Fig. 8. Finally, it has to be noted that, according to the chemical analysis of

the sample, no hydroxyl groups are present (see Sec. III A). Nevertheless strong proton ENDOR signals were detected. This has to be explained by the high sensitivity of ENDOR compared to the techniques used for the chemical analysis of the sample, when the protons are in the near vicinity of the paramagnetic centers.

### D. The Z1 radical

In addition to the A5 signal, another strong EPR signal is visible, i.e., the Z1 signal. A signal with exactly the same principal  $g$  tensor values has already been studied intensively with ENDOR in hydroxyapatites, precipitated from an aqueous solution.<sup>25</sup> From this study, it was deduced that the center had to be ascribed to a  $CO_3^{3-}$  radical located at a B site, with a vacancy on the nearest hydroxyl site. ENDOR measurements performed on the Z1 signal observed in the sample studied in this paper, resulted in the same conclusions. This is not surprising as we assume that we are dealing with the same radical. Thus the precursor of the  $CO_3^{3-}$  Z1 radical is thought to be incorporated by the following substitution mechanism:<sup>25</sup>



## VI. CONCLUSIONS

In the present work, a hydroxyapatite sample synthesized at high temperatures has been examined with EPR and ENDOR. The sample contains carbonate groups located at both hydroxyl and phosphate sites.

The two strongest EPR signals were assigned to  $O^-$  and  $CO_3^{3-}$  radicals.  $^{31}P$  and  $^1H$  ENDOR powder spectra were recorded for the  $O^-$  ion for different magnetic field settings. Interactions with three inequivalent sets of  $^{31}P$  nuclei and with one set of protons were resolved in the spectra. The computer analysis of the spectra, based on the "orientation-selection" principle, unambiguously made clear that the  $O^-$  radical is located at a hydroxyl site, with a vacancy on the nearest hydroxyl site.

By plotting the amplitude of the  $O^-$  EPR signals versus the A type carbonate content of a series of related samples, a positive correlation is found, indicating that the precursor of the  $O^-$  ion most probably is a carbonate group. In addition, the presence of the vacancy can only be explained by assuming a carbonate group as a precursor for the  $O^-$  ion. In this way, a complete and detailed model for the  $O^-$  ion in the studied carbonated hydroxyapatite sample could be obtained.

## ACKNOWLEDGMENTS

The authors wish to express their gratitude to Dr. F. Driessens of the Catholic University of Nijmegen (The Netherlands) for providing the samples. The "Executieve van de Vlaamse Gemeenschap-Departement Onderwijs" is gratefully acknowledged for financial support. The NFSR (Belgium) is acknowledged for support.

- <sup>1</sup>F. C. M. Driessens and R. M. H. Verbeeck, *Biomaterials* (CRC, Boca Raton, 1990).
- <sup>2</sup>P. Cevc and M. Schara, *Radiat. Res.* **51**, 581 (1972).
- <sup>3</sup>K. Ostrowski, A. Dziedzic-Goclawska, W. Stachowicz, and J. Michalik, *Clin. Orthop.* **97**, 213 (1973).
- <sup>4</sup>R. A. Peckauskas and I. Pullman, *Calcif. Tissue Res.* **25**, 37 (1973).
- <sup>5</sup>R. Sato, *Calcif. Tissue Int.* **29**, 95 (1979).
- <sup>6</sup>G. Cevc, P. Cevc, M. Schara, and U. Scaleric, *Nature* **286**, 425 (1980).
- <sup>7</sup>H. J. Tochon-Danguy, M. Geoffroy, and C. A. Baud, *Arch. Oral Biol.* **25**, 357 (1980).
- <sup>8</sup>Y. Doi, T. Aoba, M. Okazaki, J. Takahashi, and Y. Moriwaki, *Calcif. Tissue Int.* **33**, 81 (1981).
- <sup>9</sup>Y. Doi, Y. Moriwaki, T. Aoba, M. Okazaki, J. Takahashi, and K. Joshin, *J. Dent. Res.* **61**, 429 (1982).
- <sup>10</sup>M. Geoffroy and H. J. Tochon-Danguy, *Calcif. Tissue Int.* **34**, S99 (1982).
- <sup>11</sup>M. Geoffroy and H. J. Tochon-Danguy, *Int. J. Radiat. Biol.* **48**, 621 (1985).
- <sup>12</sup>F. J. Callens, R. M. H. Verbeeck, P. F. A. Matthys, L. C. Martens, E. R. Boesman, and F. C. M. Driessens, *Bull. Soc. Chim. Belg.* **95**, 589 (1986).
- <sup>13</sup>F. J. Callens, R. M. H. Verbeeck, P. F. A. Matthys, L. C. Martens, and E. R. Boesman, *Bull. Soc. Chim. Belg.* **96**, 165 (1986).
- <sup>14</sup>F. J. Callens, R. M. H. Verbeeck, D. E. Naessens, P. F. A. Matthys, and E. R. Boesman, *Calcif. Tissue Int.* **44**, 114 (1989).
- <sup>15</sup>F. J. Callens, R. M. H. Verbeeck, D. E. Naessens, P. F. A. Matthys, and E. R. Boesman, *Calcif. Tissue Int.* **48**, 249 (1991).
- <sup>16</sup>P. Moens, F. Callens, P. Matthys, F. Maes, R. Verbeeck, and D. Naessens, *J. Chem. Soc. Faraday Trans.* **87**, 3137 (1991).
- <sup>17</sup>P. D. W. Moens, R. M. H. Verbeeck, P. J. De Volder, F. J. Callens, and E. A. P. De Maeyer, *Calcif. Tissue Int.* **53**, 416 (1993).
- <sup>18</sup>F. J. Callens, R. M. H. Verbeeck, D. E. Naessens, P. F. A. Matthys, and E. R. Boesman, *Calcif. Tissue Int.* **53**, 386 (1993).
- <sup>19</sup>N. M. Atherton, *Principles of Electron Spin Resonance* (PTR Prentice Hall, London, 1993).
- <sup>20</sup>G. C. Hurst, T. A. Henderson, and R. W. Kreilick, *J. Am. Chem. Soc.* **107**, 7294 (1985).
- <sup>21</sup>T. A. Henderson, G. C. Hurst, and R. W. Kreilick, *J. Am. Chem. Soc.* **107**, 7299 (1985).
- <sup>22</sup>S. P. Greiner and R. W. Kreilick, *J. Magn. Reson.* **100**, 43 (1992).
- <sup>23</sup>J. Hüttermann, in *EMR of Paramagnetic Molecules*, edited by L. J. Berliner and J. Rueben, *Biological Magnetic Resonance* Vol. 13 (Plenum, New York, 1994).
- <sup>24</sup>H. Van Willigen, A. H. Roufosse, and M. J. Glimcher, *Calcif. Tissue Int.* **31**, 70 (1980).
- <sup>25</sup>P. D. Moens, F. J. Callens, P. F. Matthys, and R. M. Verbeeck, *J. Chem. Soc. Faraday Trans.* **90**, 3137 (1994).
- <sup>26</sup>P. D. W. Moens, F. J. Callens, E. R. Boesman, and R. M. H. Verbeeck, *Appl. Magn. Reson.* **9**, 103 (1995).
- <sup>27</sup>J. A. Weil, J. R. Bolton, and J. E. Wertz, *Electron Paramagnetic Resonance: Elementary Theory and Practical Applications* (Wiley, New York, 1994).
- <sup>28</sup>J. R. Pilbrow, *Transition Metal Ion Electron Spin Resonance* (Clarendon, Oxford, 1990).
- <sup>29</sup>G. Rist and J. Hyde, *J. Chem. Phys.* **52**, 4532 (1970).
- <sup>30</sup>F. C. M. Driessens, R. M. H. Verbeeck, and J. H. M. Heijligers, *Inorg. Chim. Acta* **504**, 195 (1983).
- <sup>31</sup>M. I. Kay, R. A. Young, and A. S. Posner, *Nature* **204**, 1050 (1964).
- <sup>32</sup>P. Moens, P. De Volder, R. Hoogewijs, F. Callens, and R. Verbeeck, *J. Magn. Reson. A* **101**, 1 (1993).
- <sup>33</sup>M. Mengeot, R. H. Bartram, and O. R. Gilliam, *Phys. Rev. B* **11**, 4110 (1975).
- <sup>34</sup>J. R. Brailsford and J. R. Morton, *J. Chem. Phys.* **51**, 4794 (1969).